Cell
PRESS

Structural Insights into Rcs Phosphotransfer: The Newly Identified RcsD-ABL Domain Enhances Interaction with the Response Regulator RcsB

Kerstin Schmöe,[1] Vladimir V. Rogov,[1,2] Natalia Yu. Rogova,[1] Frank Löhr,[1] Peter Güntert,[1,3] Frank Bernhard,[1] and Volker Dötsch[1,*]

[1]Institute of Biophysical Chemistry and Center for Biomolecular Magnetic Resonance, Goethe University, Max-von-Laue-Strasse 9, 60438 Frankfurt/Main, Germany
[2]Institute of Protein Research, 142290 Pushchino, Russia
[3]Frankfurt Institute for Advanced Studies, Ruth-Moufang-Strasse 1, 60438 Frankfurt/Main, Germany
*Correspondence: vdoetsch@em.uni-frankfurt.de
DOI 10.1016/j.str.2011.01.012

SUMMARY

The Rcs-signaling system is one of the most remarkable phosphorelay pathways in *Enterobacteriaceae*, comprising several membrane-bound and soluble proteins. Within the complex phosphotransfer pathway, the histidine phosphotransferase (HPt) domain of the RcsD membrane-bound component serves as a crucial factor in modulating the phosphorylation state of the transcription factor RcsB. We have identified a new domain, RcsD-ABL, located N terminally to RcsD-HPt that interacts with RcsB as well. We have determined its structure, characterized its interaction interface with RcsB, and built a structural model of the complex of the RcsD-ABL domain with RcsB. Our results indicate that the effector domain of RcsB, which normally binds to DNA, is recognized by RcsD-ABL, whereas the HPt domain interacts with the phosphoreceiver domain of RcsB.

INTRODUCTION

Bacteria live in habitats with frequently changing environmental conditions and, consequently, have developed elaborate strategies to survive. To obtain information about changes in the environment, bacteria use a whole array of membrane-bound receptors that transfer information to the cellular interior by a phosphorylation cascade. These phosphotransfer pathways are referred to as two-component systems (West and Stock, 2001) and usually involve two proteins: a membrane-bound sensor histidine kinase (HK), and a cytoplasmic-response regulator. After receiving an external stimulus, for example, via a signal recognition domain, the signal response is generated by autophosphorylation of a conserved histidine residue in the HK domain. Subsequently, this phosphoryl group is transferred to a conserved aspartic acid in the phosphoreceiver (PR) domain of a response regulator, usually a soluble transcription factor in the cytoplasm. The phosphorylation of this aspartic acid leads to conformational changes in the effector domain, followed by binding to specific promoter regions on the DNA (Stock et al.,
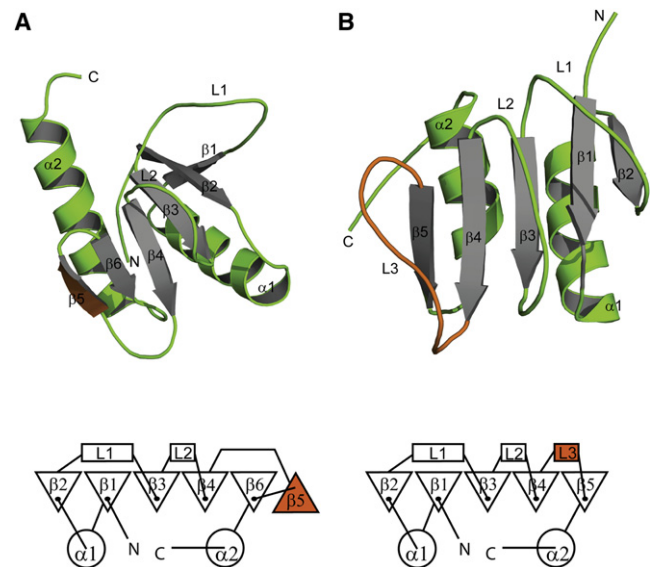
1989). An additional regulatory level is the requirement for most transcription factors and HKs to form homodimers (and also heterodimers in the case of some transcription factors) to interact effectively with the DNA or to promote the phosphorelay (Clarke et al., 2002; Khorchid et al., 2005; Maris et al., 2005; Tomomori et al., 1999; Wehland et al., 1999). Prominent examples for such two-component systems are the EnvZ/OmpR (Egger et al., 1997) and FixL/FixJ (Nixon et al., 1986) systems. Besides the basic two-component systems, more complex HKs exist that contain in addition to the HK domain a PR domain and a histidine phosphotransferase (HPt) domain, which can also exist as a separate protein (Dutta et al., 1999). These so-called hybrid sensor kinases contain multiple phosphodonor and acceptor sites and use multistep phosphorelay schemes mediated by a His-Asp-His-Asp cascade rather than promoting a single phosphotransfer. They likely provide advantages such as increasing the variety of signaling strategies, allowing greater levels of control, and more checkpoints for the input of information (Grebe and Stock, 1999; Zhang and Shi, 2005). Some prominent examples are the multistep phosphorelays of Sln1-Ypd1-Ssk1 from *S. cerevisiae* (Zhao et al., 2008) and of KinA-Spo0F-Spo0B-Spo0A from *B. subtilis* (Stephenson and Hoch, 2002; Varughese et al., 2006; Zapf et al., 2000), as well as the ArcB/ArcA (Iuchi, 1993; Iuchi and Lin, 1992) and BvgS/BvgA (Uhl and Miller, 1996) systems. Especially for the KinA-Spo0F-Spo0B-Spo0A phosphorelay, many kinases and phosphatases have been discovered that clearly demonstrate the additional level of control (Krell et al., 2010). Among multistep phosphorelays, the highly complex regulator system Rcs is unique. Originally believed to be a *r*egulator of *c*apsule synthesis in *Enterobacteriaceae*, the Rcs phosphorelay has also been found to be involved in transcriptional networks in cell division, motility, biofilm formation, and virulence (Majdalani and Gottesman, 2005). Recently, the Rcs phosphorelay has been implicated in the peptidoglycan stress response induced either by β-lactam antibiotics or by exposure to lysozyme followed by regulation of expression of lysozyme inhibitors (Callewaert et al., 2009; Laubacher and Ades, 2008). However, the exact stimulus of this complex pathway is still unknown. Therefore, investigation of the regulatory mechanisms of the phosphorelay is of particular importance. Contrary to classical two-component systems, the Rcs-signaling pathway in *E. coli*
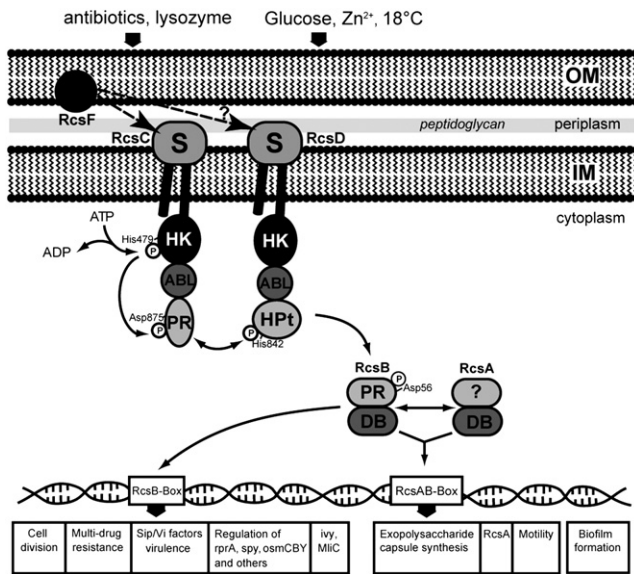
Figure 1. Scheme of the Rcs Phosphorelay System in *E. coli*
It comprises the components RcsF, RcsC, RcsD, RcsB, and RcsA. After the Rcs system has been activated by an external stimulus, probably via the lipoprotein RcsF, the hybrid sensor HK RcsC autophosphorylates via a conserved histidine residue. As indicated by the arrows, the phosphoryl group is transferred to the PR domain RcsC-PR and from there to the HPt domain of the protein RcsD. Finally, the phosphoryl group is transferred to the transcription factor RcsB. RcsB can either interact alone with the DNA via the RcsB-Box or in complex with RcsA via the RcsAB-Box. In contrast to RcsC, RcsD does not show autophosphorylation activity because the active site histidine residue is missing.

Figure 2. Comparison of the Structures of RcsD-ABL and RcsC-ABL
The ribbon diagrams of the RcsD-ABL (PDB ID 2KX7) (A) and RcsC-ABL (PDB ID 2AYY) (B) structures are shown in the same orientation. The major structural differences—β strand β5 in RcsD-ABL and loop L3 in RcsC-ABL—are shown in orange. A schematic representation of the secondary structure organization of both proteins is shown below the structures. Additional information is available in Figures S1 and S2.

involves a His-Asp-His-Asp cascade (Figure 1) (Chen et al., 2001) and is composed of the five proteins RcsF, RcsC, RcsD, RcsB, and RcsA. The outer membrane protein RcsF is described as a lipoprotein involved in activation of RcsC (Castanie-Cornet et al., 2006; Majdalani et al., 2005). After activation, the signal is passed on to the sensor domains of the membrane-bound RcsC and/or RcsD proteins. The hybrid sensor kinase RcsC gets autophosphorylated at His479 before the phosphoryl group is transferred to Asp875 in its PR domain. From here, the phosphoryl group is transferred to His842 in the HPt domain of RcsD, which cannot autophosphorylate because its kinase domain does not contain the canonical active site histidine (Takeda et al., 2001) (Figure 1). The HPt domain facilitates the transfer of the phosphoryl group from RcsD to the conserved aspartic residue Asp56 of the PR domain of the transcription factor RcsB. Depending on its phosphorylation state, RcsB binds either alone to the DNA or together with the accessory protein RcsA to the RcsAB box motif (Pristovsek et al., 2003; Wehland and Bernhard, 2000). The Rcs system has been intensively investigated by microbiological and mutational analysis. In contrast, many aspects of the structural organization of this system and its phosphotransfer reactions still have to be investigated. Recently, we reported the structures of the RcsD-HPt domain (Rogov et al., 2004), the RcsC-PR domain, and of the novel RcsC-ABL domain (Rogov et al., 2006). Here, we focus on the interface between RcsD and RcsB and report the discovery of the new domain RcsD-ABL, located N terminally to the HPt domain. We

present the structure of this domain determined by liquid-state NMR spectroscopy and demonstrate that it interacts with RcsB. In addition we characterize the complex via analysis of chemical shift perturbations. We also compare the binding properties of RcsD-HPt and RcsD-ABL to RcsB, which provides insight into the function of the newly discovered domain RcsD-ABL.

RESULTS

Identification and Structure Determination of RcsD-ABL
Analysis of the linker region between the HK and HPt domains of RcsD indicated the presence of a, so far, unknown structural region (residues 688–795). Secondary structure predictions in this region suggested the existence of both β strands and α helices. In order to characterize this potentially structured domain, we expressed it in *E. coli* and determined the three dimensional structure of this 13.3 kDa domain by liquid-state NMR spectroscopy (Figure 2A). The statistics are summarized in Table 1. The central structural element of the protein is a β sheet composed of six β strands with a β2-β1-β3-β4-β6-β5 topology. The β sheet is surrounded by two α helices: α1 and α2. Interestingly, the β strand β5 has an antiparallel orientation, whereas all other β strands form a parallel β sheet. This antiparallel β strand β5 contains charged arginine and glutamate residues, whereas the other five β strands are predominantly hydrophobic. In some of the calculated structures for RcsD-ABL, the loop L2 contains also a small 3_{10}-helical section, including residues S741 and N742 following Pro 740. In analogy to the recently discovered ABL domain of RcsC, which was found to be an

Table 1. Structural Statistics of 25 Energy-Minimized Conformers of RcsD-ABL

Input Restraint Statistics	
Total number of meaningful distance restraints	1672 (82)[a]
Intraresidual (i = j)	190
Sequential (|i − j| = 1)	414
Medium range (1 < |i − j| < 4)	412 (44)[a]
Long range (|i − j| > 4)	656 (38)[a]
Restraint violations in DYANA ensemble (50 conformers) total	0.0
Maximal violations (A)	0.0
Restraint Statistics in Final Ensemble	
Rmsd from experimental restraints	0.0118 ± 0.0013
Distance (A)	0.3160 ± 0.0660
Angle (°)	0.0033 ± 0.0001
Rmsd from idealized covalent geometry	
Bond lengths (A)	0.4320 ± 0.0150
Bond angles (°)	1.1050 ± 0.1100
Improper angles (°)	89.1
PROCHECK Ramachandran plot analysis (%)[b]	
Residues in most favored regions	
Residues in additional regions	7.6
Residues in generously allowed regions	1.6
Residues in disallowed regions	1.6
Structural precision, rmsd (A) to mean structure	
Backbone atoms (residues 696–790)[c]	0.58 ± 0.08
All heavy atoms (residues 696–790)	0.97 ± 0.08

[a] The number of included H-bond restraints is indicated in parentheses.
[b] Values for the structured part only (696–790).
[c] N, C$^{\alpha}$, and C′.

independent structural domain with a new α/β organization (Rogov et al., 2006), we named this new domain RcsD-ABL (α/β/loop).

To classify the fold of RcsD-ABL, we performed a structural similarity search using DALI and identified about 560 different structures with homology to RcsD-ABL. Most of the homologous structures belong to the flavodoxin-like fold, which consists of a five-stranded parallel β sheet sandwiched between two α-helical layers. This is the classical fold for response-regulator PR domains represented by the CheY-like superfamily. However, RcsD-ABL diverges from this classical PR domain fold by the presence of the sixth β strand, which replaces α helix α3 of a typical PR domain, and furthermore, by the replacement of α helices α1 and α2 with the loops L1 and L2.

## Comparison of the RcsD-ABL and RcsC-ABL Domains

Recently, we identified RcsC-ABL as a folded domain of RcsC (Rogov et al., 2006). Figure 2 shows a comparison of the structures of the RcsD-ABL and RcsC-ABL domains. Both proteins are of similar size (RcsD-ABL: 13.3 kDa, residues 688–795; RcsC-ABL: 12 kDa, residues 705–805) and are located C terminal to their respective HK domains. Both structures consist of a central β sheet with two α helices located on one side (the five central β strands and the first α helix can be superimposed with an rmsd value of 1.43 Å) (see Figure S1 available online). However, both structures differ in the number of β strands. As described above, RcsD-ABL contains five parallel β strands with a sixth β strand (β5) attached in an antiparallel orientation to β strand β6. The existence of a sixth antiparallel β strand is, so far, unique within the CheY super family. In RcsC-ABL this antiparallel β strand is replaced with the loop L3 connecting β4 and β5 (Figures 2 and 3). An important similarity between RcsC-ABL and RcsD-ABL is that the aspartic residue that forms the active site, and that accepts the phosphoryl group in classical PR domains, is missing, suggesting that it is unlikely that these ABL domains act as PR domains.

To search for other potential ABL domains, we screened the GenBank database for sequences homologous to RcsD-ABL. This search resulted in 20 entries with high similarity, all of which belong to potential sensor kinases from *Enterobacteriaceae*. The alignment of these potential ABL sequences from different species revealed a high conservation, except for the antiparallel-oriented β strand β5, which does not show any significant conservation. A comparable alignment of all potential ABL sequences with the RcsC-ABL sequence from *E. coli* shows only low conservation in the primary sequence (Figure 3).
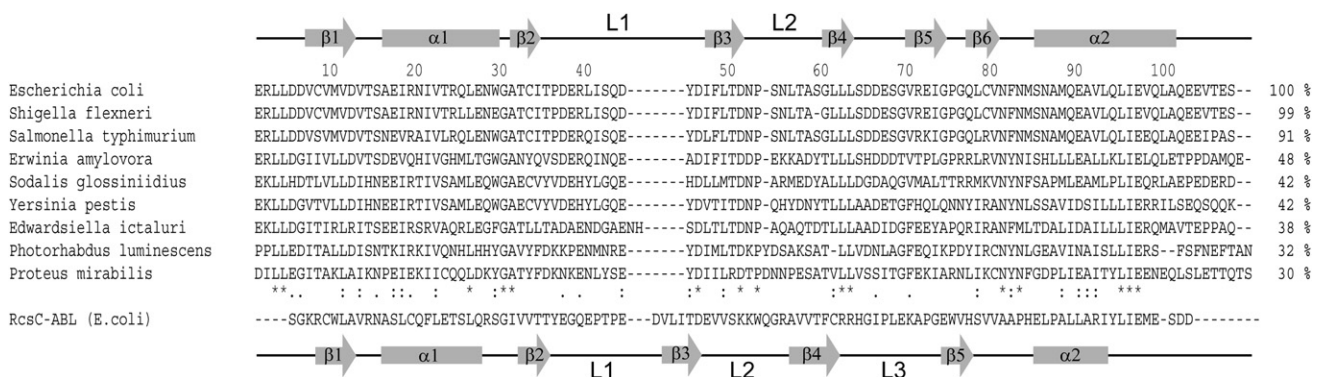
Figure 3. Sequence Alignment of Domains with Homology to RcsD-ABL from Different Species of *Enterobacteriaceae* with the Sequence of *E. coli* RcsC-ABL
Secondary structure elements and loops determined in this work for the *E. coli* RcsD-ABL are shown on top of the alignment. The sequence of RcsC-ABL and its secondary structure elements are shown at the bottom.
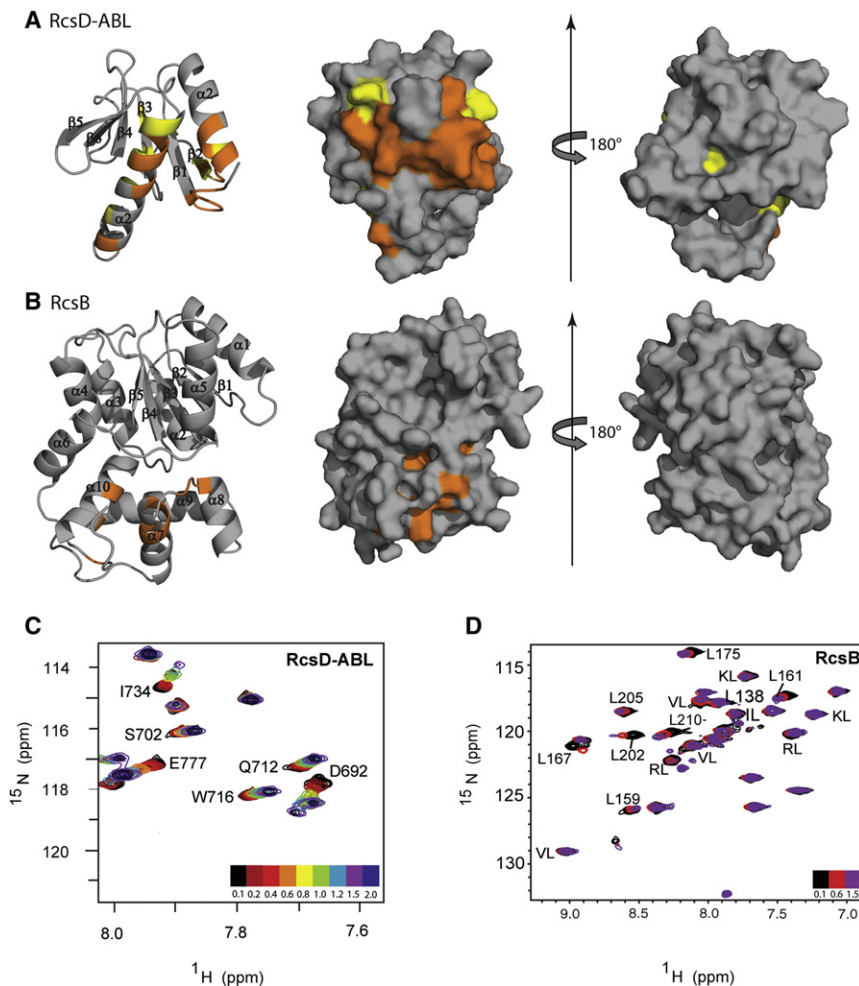
Figure 4. Mapping of the RcsD-ABL:RcsB-Binding Site

In (A), a ribbon diagram and a surface representation are shown for RcsD-ABL, and in (B), the corresponding representations are shown for RcsB. For RcsD-ABL all residues with shifts >0.17 ppm are colored in orange, and those with shifts between 0.17 and 0.08 ppm are labeled in yellow. For RcsB all residues that showed differences in chemical shift and could be identified by the HNCO experiments are labeled in orange. Structures shown on the right were obtained by 180° rotation of the structures shown on the left. In (C), a selective area of a multiple overlay of 2D ^{15}N-^{1}H-TROSY-HSQC spectra obtained from the titration of RcsD-ABL (0.2 mM) with increasing concentration of RcsB (0.02–0.4 mM) is shown. (D) The corresponding titration experiments of RcsB (0.2 mM) with increasing concentration of RcsD-ABL (0.02–0.3 mM). RcsB was selectively labeled with ^{15}N leucine. Amino acid pairs that could be identified by HNCO experiments are indicated. In both (C) and (D), the molar ratios are indicated in different colors (from 1: 0.1 to 1:2). Additional information is available in Figures S3–S5.

component systems with homology to members of the LuxR family. It consists of a typical N-terminal PR domain with an α/β sandwich fold, the conserved aspartic residue Asp56 in the active center, and a C-terminal effector domain with a helix-turn-helix DNA-binding motif (Kahn and Ditta, 1991; Pristovsek et al., 2003; Robinson et al., 2000). Unfortunately, so far, the full structural characterization of RcsB was not possible. While crystallization experiments have not been successful, only 60% of the residues, mainly in the C-terminal DNA-binding domain, could be assigned by NMR spectroscopy. Nevertheless the structure of the DNA-binding domain of the highly homologous RcsB protein from *E. amylovora* (Pristovsek et al., 2003) (but not of its PR domain) has been determined. To be able to interpret NMR-based titration experiments between the *E. coli* RcsB protein and the RcsD-ABL domain, we built a homology model of RcsB based on the DNA-binding domain from *E. amylovora* RcsB and on the PR domain of the homologous transcription factor NarL (Baikalov et al., 1996) (Figure S3). To characterize the interaction interface in the RcsD-ABL:RcsB complex, we first carried out NMR titration experiments with ^{15}N-labeled RcsD-ABL and unlabelled RcsB. Figure 4C shows an overlay of several titration steps, indicating that both proteins interact with each other and that this interaction is in fast exchange on the NMR timescale. Mapping the chemical shift differences onto the structure of RcsD-ABL demonstrated that the interaction interface includes the C-terminal end of helix α1, the following strand β2, and large parts of helix α2 (Figure 4A).

To confirm the importance of the identified binding interface, we created the triple mutation N715A, Q776A, L780A. Investigating the interaction of this mutant with RcsB by isothermal

It has been speculated that RcsC and RcsD form a heterodimeric unit (Takeda et al., 2001). To investigate if this heterodimerization is promoted by the ABL domains of both proteins, we carried out NMR titration experiments with the isolated RcsC-ABL and RcsD-ABL domains. However, these experiments did not provide any evidence for interaction between the ABL domains (Figure S2). Further interaction studies also indicated no interaction of the RcsD-ABL domain and the PR domain of RcsC or the HPt domain of RcsD. Interaction studies with the HK domains could not be carried out because expression of these domains in high amounts was not possible. The results obtained so far do not support a model in which the RcsD-ABL domain promotes domain-domain interaction within RcsD or between RcsD and RcsC.

Interaction of RcsD-ABL and RcsB—Characterization of the Binding Interfaces

RcsD interacts not only with RcsC but also with the transcriptional regulator RcsB, which controls more than 150 different genes in *E. coli* (Hagiwara et al., 2003). NMR titration experiments of the RcsD-ABL domain showed interaction with RcsB. RcsB is a classical transcription factor of bacterial two-

titration calorimetry (ITC) showed a more than 10-fold increase of the dissociation constant compared with the wild-type protein (Figure S4). Detailed analysis revealed that the signs of both the binding enthalpy and entropy changed relative to wild-type RcsD-ABL. Thus, binding of the mutant is entropy driven, characteristic for the replacement of polar interactions with hydrophobic ones.

We further wanted to analyze the interaction interface of RcsB with RcsD-ABL and used for this investigation the homology model mentioned above. Extensive optimization of buffer conditions allowed us to increase the number of peaks detectable in [^{15}N, ^{1}H]-TROSY-HSQC spectra to 80%; however, in triple resonance experiments the number of peaks observed was still quite low. Therefore, we used a fast mapping protocol in combination with the homology model to examine the interface without knowing the full backbone assignment of the protein (Reese and Dotsch, 2003). Briefly, RcsB was selectively ^{15}N labeled with the hydrophobic amino acids valine, leucine, isoleucine, phenylalanine, or tyrosine. The labeling was achieved with the strain DL39, which is auxotrophic for the aforementioned amino acids. To map the interface on RcsB, we recorded [^{15}N, ^{1}H]-TROSY-HSQC spectra with increasing concentrations of RcsD-ABL (from a molar ratio of 1:0.1 to 1:1 in five steps). The spectra were recorded under the same conditions as for the ^{15}N-RcsD-ABL/RcsB titration experiments (0.2 mM RcsB sample in 50 mM Na$_2$HPO$_4$, 100 mM NaCl [pH 6.7]). In this way we could visualize 30% of the protein without overlap problems. We were able to observe signals for all 14 valine residues, for 24 of 29 leucines, for 18 out of 20 isoleucines, for five out of six phenylalanines, and for all four tyrosines. Differences in the chemical shifts between free RcsB and its complex with RcsD-ABL were observed for all five selected amino acid types. To unambiguously identify some of those signals that show chemical shift changes, we recorded several 2D [^{15}N, ^{1}H]-TROSY-HNCO spectra with samples selectively 1-^{13}C- and ^{15}N-labeled amino acids, which allowed one to assign pairs of a ^{13}C-labeled amino acid directly followed by a ^{15}N-labeled one. Figure 4D shows a representative [^{15}N, ^{1}H]-TROSY-HSQC spectrum of RcsB labeled with ^{15}N-leucine, where nearly all leucine residues with differences in chemical shift could be identified by recording HNCO spectra of RcsB with selectively ^{13}C and ^{15}N-labeled amino acid combinations. The results are summarized in Figure S5. In this way we could identify the interaction interface of RcsB with RcsD-ABL in its effector domain, the DNA-binding domain. We could confirm this assignment by comparison with the [^{15}N, ^{1}H]-TROSY-HSQC spectrum of the highly homologous DNA-binding domain of *E. amylovora,* for which a complete backbone assignment is available. These results indicate that the interaction with the ABL domain is centered on helix α10 of the DNA-binding domain and additionally involves helix α7 and small parts of helix α8 (Figure 4B).

In Vivo Interaction of RcsD-ABL with RcsB Determined by β-Galactosidase Activity

The interaction of RcsD-ABL with RcsB suggested that RcsD-ABL might be an interaction domain that is important for binding of RcsB to RcsD. Therefore, overproduction of RcsD-ABL in *E. coli* should disrupt the phosphorelay pathway. Based on this
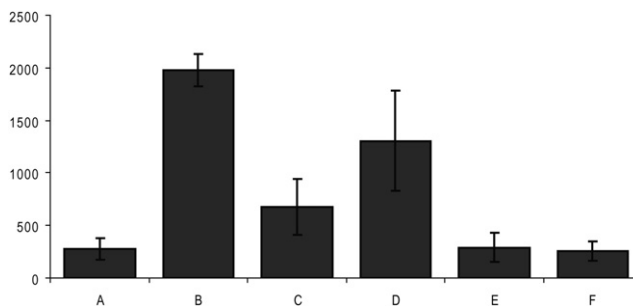
Figure 5. Effect of Overexpression of RcsD-ABL in *E. coli* on the Transcriptional Activity of RcsB on the *rprA:lacZ* Reporter Gene as Determined by β-Galactosidase Activity

Data are given in Miller units and were repeated in triplicate. The error bars represent standard deviations.

(A) Wild-type DH300 cells.

(B) Treatment with the antibiotic mecillinam.

(C) DH300 cells transformed with a plasmid containing RcsD-ABL induced with IPTG in the presence of mecillinam.

(D) DH300 cells transformed with a plasmid containing RcsD-ABL but without induction.

(E) and (F) are the same as (C) and (D) but without treatment with the antibiotic.

assumption, we analyzed the influence of RcsD-ABL expression on the transcriptional activity of RcsB by performing a β-galactosidase assay (Miller, 1972). We used the strain DH300, which contains the rprA-lacZ insert. Because the binding of RcsB to the rprA promoter is independent of RcsA, we were able to investigate the RcsB/ RcsD-ABL interaction without interference from RcsA. To activate the RcsB pathway that should lead to a higher transcriptional activity of RcsB and a concomitant increase in the β-galactosidase activity, we used the antibiotic mecillinam (Laubacher and Ades, 2008). First, *E. coli* DH300 cells were incubated with or without overexpression of RcsD-ABL with 0.3 μg/ml antibiotic for 1 hr at 37°C, after which the β-galactosidase test was performed with ONPG as a substrate. Wild-type *E. coli* DH300 showed a 9-fold increase in the β-galactosidase signal when activated with mecillinam. Induction of the RcsD-ABL plasmid with IPTG (1 mM) in the presence of mecillinam decreased the activity by 70% compared with the wild-type (Figure 5). These results complement and support the proposed interaction of RcsB with RcsD-ABL in vivo.

Binding of RcsB to RcsD-ABL Enhances the Interaction between the RcsD-HPt and the RcsB-PR Domains

The experiments described above show that the RcsD-ABL domain interacts with the DNA-binding domain of RcsB. However, both domains are only indirectly involved in the phosphoryl transfer, probably by helping to form a complex between the RcsD-HPt domain and the RcsB-PR domain. Therefore, the phosphoryl-transfer complex most likely consists of the ABL and the HPt domain of RcsD and the PR and DNA-binding domain of RcsB. To investigate these additional interactions, we performed NMR titration experiments and ITC measurements with unlabelled RcsB and the three ^{15}N-labeled constructs RcsD-ABL, RcsD-HPt, and the bidomain RcsD-ABL-HPt. The backbone amide resonances of the bidomain RcsD-ABL-HPt were assigned with the program AutoAssign (Moseley et al., 2001)

based on the data of the individual domains, whereas the linker was assigned manually. In contrast to the titration experiments with the single protein constructs RcsD-ABL (reported above) and RcsD-HPt (reported previously [Rogov et al., 2004]) that showed fast exchange behavior, interaction of RcsB with the RcsD-ABL-HPt bidomain construct was in intermediate exchange, as suggested by significantly broadened resonances (Figure 6B). Furthermore, the binding interface on the bidomain differed slightly from the sum of the interfaces on the two individual domains. In the bidomain this interface included the linker region (residues Q789–D800).

The titration experiments reported above suggested that both the ABL and the HPt domains interact with RcsB and specifically that the ABL domain binds to the DNA-binding domain, and the HPt domain interacts with the PR domain of RcsB, which is further supported by the fact that the HPt and the PR domains are involved in the phosphoryl transfer. To further investigate this interaction, we performed again a fast mapping experiment with amino acid type selectively labeled RcsB and the RcsD-HPt domain. Although in the titration experiments with the RcsD-ABL domain we detected large chemical shift differences, we could detect only small differences in the titration experiments with the isolated RcsD-HPt domain, mainly located in the RcsB-PR domain. This result confirms the suggested model that the DNA-binding domain of RcsB interacts with the RcsD-ABL domain, whereas the HPt domain binds to the PR domain.

To obtain quantitative binding data, we performed ITC measurements at two different temperatures. The results are summarized in Figure 6A and Table 2. RcsD-ABL bound to RcsB with a dissociation constant of ~2 μM, whereas the binding constant for the HPt domain was ~40 μM. Repeating the experiment with the bidomain RcsD-ABL-HPt resulted in a value of ~10 μM using a one-site binding model for data analysis. This surprisingly weaker binding of the bidomain and the observation that the NMR experiments indicated stronger interaction prompted us to analyze the ITC data with a two-binding site model. This analysis showed that the interaction between the RcsD-ABL domain and RcsB basically does not change, whereas the interaction between the RcsD-HPt domain and RcsB becomes significantly stronger (~8 μM). In combination with the NMR titration data, these results suggest that the interaction between the RcsD-ABL domain and the DNA-binding domain of RcsB provides an important bridge between RcsD and RcsB that enhances the interaction between the PR and the HPt domains that are directly involved in the phosphoryl-transfer reaction.

DISCUSSION

In this article we report the identification of a new domain, named RcsD-ABL, in the membrane protein RcsD. This newly characterized domain is located N terminally to the HPt domain of RcsD and interacts with the effector domain of the transcription factor RcsB. We have analyzed the interaction interfaces of the RcsD-HPt and RcsD-ABL domains with their downstream-interaction partner, RcsB, which consists of a DNA-binding and a PR domain. To our knowledge, RcsD is only the second example of a sensor protein providing an extra domain as a binding site for a response regulator involved in two-component systems.

In this study it became apparent that the HK CheA and the hybrid HK-like protein RcsD show a similar arrangement of domains (Figure S6). Structurally, both the RcsD-HPt and the CheA-P1 (HPt) domains show an up-down-up-down topology (Bilwes et al., 1999; Mourey et al., 2001). However, CheA-P1 serves not only as a phosphotransfer domain but also initiates via autophosphorylation the phosphotransfer cascade (Levit et al., 1999), whereas RcsD contains an extra, but inactive, HK domain and, therefore, receives the phosphoryl group from the hybrid sensor HK RcsC (Majdalani and Gottesman, 2005). Similar to RcsD, CheA provides a separate domain, the CheA-P2 domain, as additional binding site for its response regulator, CheY (McEvoy et al., 1996). However, structurally, the CheA-P2 and RcsD-ABL domains are different. As described in detail in this article, the RcsD-ABL domain consists, with exception of β strand β5, exclusively of parallel β strands and parallel α helices. In contrast the CheA-P2 domain comprises a three-stranded antiparallel β sheet and two antiparallel α helices (McEvoy et al., 1996). However, the most significant difference is the formation of the entire complex. In the case of the chemotaxis-signaling pathway, CheY consists only of a single PR domain, which interacts with CheA-P2 via the two α helices, α1 and α2, and brings the phosphoacceptor site of CheY in close proximity to the phosphorylated histidine residue on CheA-P1 (Stewart, 1997; Zhou et al., 1996). However, the RcsD-ABL domain does not directly interact with the N-terminal PR domain of RcsB but instead interacts with the C-terminal DNA-binding domain, which acts as a tether to enable interaction between the RcsB-PR and RcsD-HPt domains. This arrangement is, so far, unique among His-Asp-His-Asp signaling cascades. Furthermore, the results indicate that in turn the RcsB DNA-binding domain is bifunctional and provides interfaces for specific DNA binding as well as for protein interactions.

Based on kinetic experiments, it was suggested that CheA-P2 brings CheY in close proximity to CheA-P1 to accelerate the phosphoryl transfer. Such acceleration is crucial for the chemotaxis system, which reacts to external stimuli within 50–100 ms; whereas most other two-component systems are coupled to transcription factors that mediate changes in protein expression levels over the course of minutes to hours (Stewart and Van Bruggen, 2004). Based on our ITC and NMR titration experiments, we could show that the affinity of the RcsD-HPt domain to its response regulator RcsB is enhanced by the RcsD-ABL domain. These experiments have further revealed that the interaction affinity of RcsB to the RcsD-ABL domain is significantly stronger than to the RcsD-HPt domain (K_D ~2 versus ~40 μM), suggesting that the RcsD-ABL domain plays a crucial role in the assembly of the active phosphoryl-transfer complex.

To obtain further insight into the interaction between RcsB and RcsD, we created a model of the RcsB effector domain docked onto the RcsD-ABL domain based on the observed chemical shift changes (Figure 7). Unfortunately, lack of structural knowledge did not allow modeling of the entire four-domain complex (Figure S6). One particular problem of trying to understand the interaction of all four domains on the structural level was the inability to obtain a structure of the PR domain of RcsB. Instead, we had to use a homology model that was based on the crystal structure of the transcription factor NarL. However, the structure of NarL represents a closed conformation, which
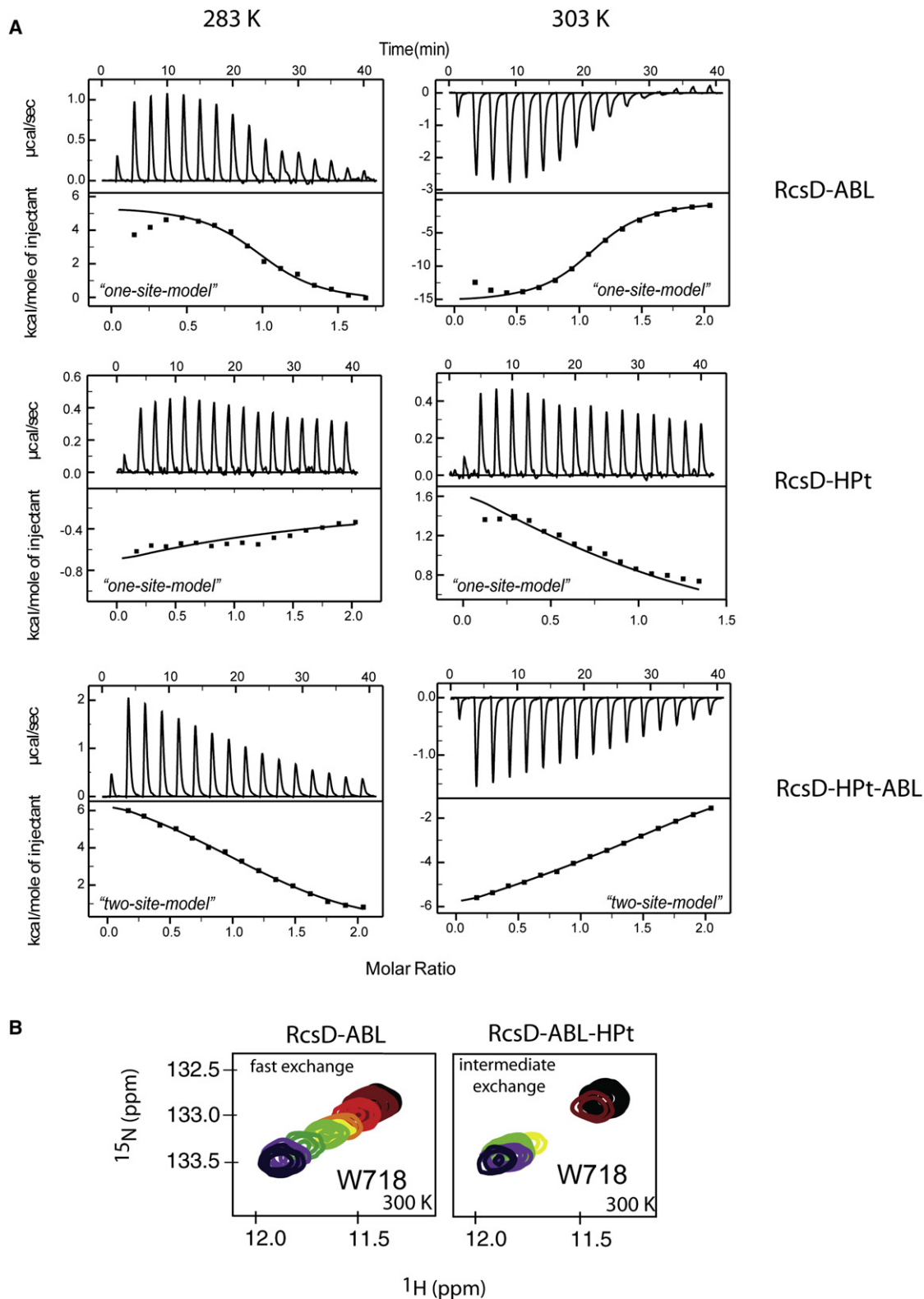
Figure 6. Comparison of Binding Affinities of RcsD-ABL and RcsD-HPt to RcsB Studied by NMR and ITC Measurements

(A) Each plot represents an ITC titration experiment performed at 283 K (left) or 303 K (right) for RcsD-ABL (top panels), RcsD-HPt (middle panels), and the bidomain RcsD-ABL-HPt (bottom panels) with RcsB. Deviations of the experimental data from the fitted curves (solid lines) are due to a monomer-dimer equilibrium of RcsB.

(B) NMR titration experiments of RcsD-ABL with RcsB indicating fast exchange on the NMR timescale (left), and of the bidomain RcsD-ABL-HPt titrated with RcsB indicating intermediate exchange (right).

Table 2. Thermodynamic Analysis of ITC Experiments Obtained at 283 and 303 K for the Interaction of RcsB with the Individual RcsD-ABL and RcsD-HPt Domains as well as with the Fused Bidomain RcsD-ABL-HPt

	283 K					
	Individual Domains RcsD-ABL, RcsD-HPt "One-site-model"		Fused Domains RcsD-ABL-HPt "One-site-model"	Fused Domains RcsD-ABL-HPt "Two-site-model"	
	RcsD-ABL	RcsD-HPt	RcsD-ABL-HPt	RcsD-ABL	RcsD-HPt
K_D (μM)	1.6	46	8.3	2.1	7.3
ΔH (kcal/mol)	+5.5 ± 0.3	+3.1 ± 0.3	+6.8 ± 0.2	+8.7 ± 3	−1.6 ± 1
	303 K					
	Individual Domains RcsD-ABL, RcsD-HPt "One-site-model"		Fused Domains RcsD-ABL-HPt "One-site-model"	Fused Domains RcsD-ABL-HPt "Two-site-model"	
	RcsD-ABL	RcsD-HPt	RcsD-ABL-HPt	RcsD-ABL	RcsD-HPt
K_D (μM)	2.2	39	12.6	4.9	8.3
ΔH (kcal/mol)	−15.5 ± 0.3	−1.8 ± 0.6	−6.4 ± 1	−10.6 ± 0.4	+1.6 ± 4

The fitting was performed with the one-site model for the single domains and with the two-site model for the RcsD-ABL-HPt bidomain.

upon phosphorylation, opens and becomes DNA-binding competent. A similar mechanism might trigger a conformational change in RcsB as well, which would lead to differences in the relative orientation of the RcsB-DNA binding domain and of the PR domain. Because we do not know the structure of the active conformation of RcsB, we have not tried to model the interaction of the RcsD-HPt and the RcsB-PR domain in the complex. Structures of complexes of HPt domains with PR domains are known from other phosphorelay systems, e.g., the Ypd1/Sln1-R1, the Spo0B/Spo0F complex (Figure S6) (Xu et al., 2003; Zhao et al., 2008), and the CheA$_3$-P1/CheY$_6$ from *R. sphaeroides* (Bell et al., 2010). However, the arrangement of four different domains in the active phosphoryl-transfer complex of the RcsC system is unique among all phosphorelay systems that have been investigated structurally so far.

The RcsC protein harbors with the RcsC-ABL domain, yet another similar domain that probably serves as an adaptor domain to enhance interaction with other, so far, unknown interaction partners. The function of the RcsC-ABL domain remains to be investigated.
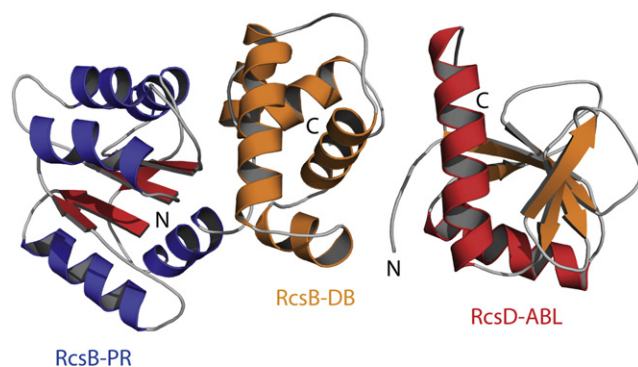
Figure 7. Model of the RcsB:RcsD-ABL Complex Obtained with the Program HADDOCK

The RcsD-ABL domain, RcsB DNA-binding domain, and RcsB-PR domain are labeled. Only the RcsD-ABL and the DNA-binding domains of RcsB were used in the docking calculations. The structure of RcsB is a homology model based on the structure of the closed conformation of NarL. Additional information is available in Figure S6.

EXPERIMENTAL PROCEDURES

Cloning Procedures

All cloning steps were performed following standard protocols (Rogov et al., 2004). Polymerase chain reactions were carried out using Vent$_R$ DNA Polymerase (New England BioLabs) and *Pfu* DNA Polymerase (Promega) for site-directed mutagenesis. As a template the *E. coli* strain XL1 was used.

The DNA fragment encoding the RcsD-ABL domain spanning residues 688–795 of the RcsD protein was amplified by using the oligonucleotides RcsD-ABL-up CGGCCATGGAGCGTTTACTGGATGATGTCTGCG and RcsD-ABL-low CGGAGATCTCGATTCTGTCACCTCTTCCTGCGCC as primers. The DNA fragment was cloned with the restriction enzymes NcoI and BglII into the expression vector pQE60 (QIAGEN), resulting in the plasmid pQE-RcsD-ABL, including a C-terminal His$_6$-tag.

Accordingly, a DNA fragment encoding the residues 688–890 of the RcsD protein and containing both the ABL and HPt domains was amplified with the oligonucleotides RcsD-ABLH-up CGGCCATGGAGCGTTTACTGGATGATGTCTGCG and RcsDABH-low CCCTCGAGTCACAGCAAGCTCTT. The DNA fragment was cloned with the restriction enzymes BamHI and XhoI into the expression vector pET21a (Novagen), resulting in the plasmid pET-RcsD-ABL-HPt containing an N-terminal T7 tag.

Protein Expression, Purification, and NMR Sample Preparations

For protein expression the plasmid pQE-RcsD-ABL was transformed into the *E. coli* M15[pREP4] strain. Expression of ^{15}N-labeled protein was achieved by growing *E. coli* bacteria on minimal media containing 1 g/l ^{15}NH$_4$Cl and 2 g/l unlabelled D-glucose. ^{13}C/^{15}N-doubly labeled protein was expressed on medium containing 1 g/l ^{15}NH$_4$Cl, 1 g/l of [U-^{13}C]-D-glucose, and 0.5 g/l ^{13}C glycerol. The cells were grown with intensive aeration slightly longer than the mid log phase (1.3–1.6 absorbance units at 600 nm) before IPTG was added to a final concentration of 1.0 mM. After 3 hr of induction, the cells were harvested, resuspended in buffer containing 10 mM Tris-HCl (pH 7.5), 150 mM NaCl, 5% glycerol, and lysed using a French press. The cell debris was removed by centrifugation, and the lysate was loaded onto a Ni-affinity sepharose (Amersham Pharmacia Biotech) column. The column was washed with 200 ml of the same buffer, and pure protein was eluted with a linear gradient of imidazole (20–400 mM).

The plasmid pET-RcsD-ABL-HPt was transformed into the BL21 (DE3) strain. Purification was carried out by anion exchange (50 mM Na$_2$HPO$_4$, 1 M NaCl gradient [pH 7.5]) and gelfiltration chromatography (50 mM Na$_2$HPO$_4$, 100 mM NaCl [pH 6.7]). The *E. coli* RcsC-ABL, RcsC-PR, and RcsD-HPt domains and the RcsB protein were overproduced and purified as described (Kelm et al., 1997; Rogov et al., 2004, 2006).

For the study of protein-protein interactions, samples were prepared by buffer exchange of the purified individual proteins using gel filtration with an HR16 Superdex75 column and subsequent co-concentration of the

RcsD-ABL/RcsB and RcsD-ABL-HPt/RcsB mixtures (50 mM Na$_2$HPO$_4$, 100 mM NaCl [pH 6.7]).

For the expression of selectively ^{13}C and/or ^{15}N-labeled RcsB, the auxotrophic strain DL39 was used, and purification followed the methods described above.

NMR Spectroscopy

NMR experiments to obtain resonance assignment of RcsD-ABL followed similar procedures as described (Rogov et al., 2006, 2007). Proton-proton distances for structure calculations were derived from 3D ^{13}C-separated and TROSY-type ^{15}N-separated NOESY experiments with the ^{13}C carrier position placed either in the aliphatic region, the methyl group region, or in the aromatic region. Spectra were obtained at 298 K on Bruker AVANCE spectrometers (Rheinstetten, Germany) operating at ^{1}H Larmor-frequencies of 600, 700, 800, and 900 MHz. Proton chemical shifts were referenced relative to internal DSS. The ^{15}N and ^{13}C chemical shifts were referenced indirectly using the consensus ratios (Wishart et al., 1995).

[^{15}N, ^{1}H]-TROSY-HSQC spectroscopy was used for the observation of the RcsD-ABL and RcsB interactions on a Bruker AVANCE 900 spectrometer. A reference [^{15}N, ^{1}H]-TROSY-HSQC spectrum was recorded using a freshly prepared RcsD-ABL sample; spectra of the complexes were acquired after dilution and co-concentration of RcsD-ABL with RcsB as described above. Two-dimensional [^{15}N, ^{1}H]-TROSY-HNCO spectra were measured with samples selectively 1-^{13}C and ^{15}N labeled on certain amino acid combinations to identify some amino acid sequences specifically.

The NMR spectra were processed and analyzed using the TopSpin 2.1 (Bruker BioSpin) and Sparky 3.114 (T. D. Goddard and D.G. Kneller, University of California, San Francisco, San Francisco) programs.

Structure Calculation

The NOE-based distance restraints were extracted from the 3D ^{13}C and ^{15}N-edited NOESY spectra using the CANDID module (Herrmann et al., 2002) of the CYANA (Guntert et al., 1997) program, version 1.0.5. The final structure calculation was performed using a simulated annealing protocol with torsion-angle dynamics (DYANA1.5) (Guntert et al., 1997) on the basis of 1590 unambiguous upper-limit restraints generated by CANDID. A total of 82 hydrogen bonds deduced from proton exchange data and CSI and TALOS programs were included as distance restraints (d$_{HO}$ ≤ 2.1 Å and d$_{NO}$ ≤ 3.1 Å). In addition, 125 torsion-angle constraints were included as predicted by the program TALOS on the basis of chemical shift values. For the calculation of the final structure ensemble, 200 structures were calculated in 10,000 time steps per conformer. The 50 best DYANA conformers were refined in an explicit water shell (Linge et al., 2003) using the CNS software package (Brünger et al., 1998), and 25 structures with the lowest energy (about −4700 kcal/mol) were selected for validation using PROCHECK-NMR 3 (Laskowski et al., 1996). The figures were prepared using the program PyMOL (DeLano Scientific LLC).

ITC

ITC experiments were performed at 283 and 303 K in 50 mM Na$_2$HPO$_4$ and 100 mM NaCl (pH 6.7) on a MicroCal VP-ITC device. For RcsB the concentration in the cell was 0.05 mM; for RcsD-ABL, RcsD-HPt, and RcsD-ABL-HPt, it was 0.6 mM (ratio 1:12). Data were analyzed with the standard program Origin 7 for ITC.

Upon titration of the RcsD-ABL domain into RcsB, we observed an additional process, which is centered at a molar ratio ∼0.5 and which is present both at 10°C and 30°C. We have interpreted this process as a change in the oligomeric state of RcsB (RcsB undergoes dimerization at concentrations used for ITC, shown by size-exclusion chromatography). We did not include this process into our fitting procedure; therefore, the experimental data and fitted curves deviate at the beginning.

β-Galactosidase Activity

Cultures were grown in LB medium at 310 K overnight. The cultures were diluted 1:100 with fresh LB medium and were grown until an OD$_{600}$ of 0.2. At that point the antibiotic mecillinam (Sigma-Aldrich) was added to a concentration of 0.3 μg/ml as described (Laubacher and Ades, 2008). After 60 min, the cells were harvested at 5500 rpm and resuspended in Z-buffer (100 mM sodium phosphate [pH 7.0], 10 mM KCl, 1 mM MgSO$_4$, 50 mM β-mercaptoethanol). After that, the β-galactosidase assay was performed according to standard methods (Miller, 1972).

Modeling

The homology model of RcsB was built by using the SWISS-model server in combination with the Deep Viewer (Guex and Peitsch, 1997). First, the program applied a homology model of RcsB to the DNA-binding domain of *E. amylovora* and to the transcription factor NarL separately. Both structures were then combined in an overlay in the program Deep View, and the homology model was applied manually to RcsB. The correctness of the homology model was checked with the *Protein Structure & Model Assessment Tools*, which involves What Check. The HADDOCK model was built by using the HADDOCK server (de Vries et al., 2010).

REFERENCES

Baikalov, I., Schroder, I., Kaczor-Grzeskowiak, M., Grzeskowiak, K., Gunsalus, R.P., and Dickerson, R.E. (1996). Structure of the *Escherichia coli* response regulator NarL. Biochemistry *35*, 11053–11061.

Bell, C.H., Porter, S.L., Strawson, A., Stuart, D.I., and Armitage, J.P. (2010). Using structural information to change the phosphotransfer specificity of a two-component chemotaxis signalling complex. PLoS Biol. *8*, e1000306.

Bilwes, A.M., Alex, L.A., Crane, B.R., and Simon, M.I. (1999). Structure of CheA, a signal-transducing histidine kinase. Cell *96*, 131–141.

Brünger, A.T., Adams, P.D., Clore, G.M., DeLano, W.L., Gros, P., Grosse-Kunstleve, R.W., Jiang, J.S., Kuszewski, J., Nilges, M., Pannu, N.S., et al. (1998). Crystallography and NMR system (CNS): a new software suite for macromolecular structure determination. Acta Crystallogr. D Biol. Crystallogr. *54*, 905–921.

Callewaert, L., Vanoirbeek, K.G., Lurquin, I., Michiels, C.W., and Aertsen, A. (2009). The Rcs two-component system regulates expression of lysozyme inhibitors and is induced by exposure to lysozyme. J. Bacteriol. *191*, 1979–1981.

Castanie-Cornet, M.P., Cam, K., and Jacq, A. (2006). RcsF is an outer membrane lipoprotein involved in the RcsCDB phosphorelay signaling pathway in *Escherichia coli*. J. Bacteriol. *188*, 4264–4270.

Chen, M.H., Takeda, S., Yamada, H., Ishii, Y., Yamashino, T., and Mizuno, T. (2001). Characterization of the RcsC→YojN→RcsB phosphorelay signaling

pathway involved in capsular synthesis in *Escherichia coli*. Biosci. Biotechnol. Biochem. *65*, 2364–2367.

Clarke, D.J., Joyce, S.A., Toutain, C.M., Jacq, A., and Holland, I.B. (2002). Genetic analysis of the RcsC sensor kinase from *Escherichia coli* K-12. J. Bacteriol. *184*, 1204–1208.

de Vries, S.J., van Dijik, M., and Bonvin, A.M. (2010). The HADDOCK web server for data-driven biomolecular docking. Nat. Protoc. *5*, 883–897.

Dutta, R., Qin, L., and Inouye, M. (1999). Histidine kinases: diversity of domain organization. Mol. Microbiol. *34*, 633–640.

Egger, L.A., Park, H., and Inouye, M. (1997). Signal transduction via the his-tidyl-aspartyl phosphorelay. Genes Cells *2*, 167–184.

Grebe, T.W., and Stock, J.B. (1999). The histidine protein kinase superfamily. Adv. Microb. Physiol. *41*, 139–227.

Guex, N., and Peitsch, M.C. (1997). SWISS-MODEL and the Swiss-PdbViewer: an environment for comparative protein modeling. Electrophoresis *18*, 2714–2723.

Guntert, P., Mumenthaler, C., and Wuthrich, K. (1997). Torsion angle dynamics for NMR structure calculation with the new program DYANA. J. Mol. Biol. *273*, 283–298.

Hagiwara, D., Sugiura, M., Oshima, T., Mori, H., Aiba, H., Yamashino, T., and Mizuno, T. (2003). Genome-wide analyses revealing a signaling network of the RcsC-YojN-RcsB phosphorelay system in *Escherichia coli*. J. Bacteriol. *185*, 5735–5746.

Herrmann, T., Guntert, P., and Wuthrich, K. (2002). ProteinNMR structure determination with automated NOE assignment using the new software CANDID and the torsion angle dynamics algorithm DYANA. J. Mol. Biol. *319*, 209–227.

Iuchi, S. (1993). Phosphorylation/dephosphorylation of the receiver module at the conserved aspartate residue controls transphosphorylation activity of histidine kinase in sensor protein ArcB of *Escherichia coli*. J. Biol. Chem. *268*, 23972–23980.

Iuchi, S., and Lin, E.C. (1992). Purification and phosphorylation of the Arc regulatory components of *Escherichia coli*. J. Bacteriol. *174*, 5617–5623.

Kahn, D., and Ditta, G. (1991). Modular structure of FixJ: homology of the transcriptional activator domain with the −35 binding domain of sigma factors. Mol. Microbiol. *5*, 987–997.

Kelm, O., Kiecker, C., Geider, K., and Bernhard, F. (1997). Interaction of the regulator proteins RcsA and RcsB with the promoter of the operon for amylovoran biosynthesis in *Erwinia amylovora*. Mol. Gen. Genet. *256*, 72–83.

Khorchid, A., Inouye, M., and Ikura, M. (2005). Structural characterization of *Escherichia coli* sensor histidine kinase EnvZ: the periplasmic C-terminal core domain is critical for homodimerization. Biochem. J. *385*, 255–264.

Krell, T., Lacal, J., Busch, A., Silva-Jimenez, H., Guazzaroni, M.E., and Ramos, J.L. (2010). Bacterial sensor kinases: diversity in the recognition of environmental signals. Annu. Rev. Microbiol. *64*, 539–559.

Laskowski, R.A., Rullmannn, J.A., MacArthur, M.W., Kaptein, R., and Thornton, J.M. (1996). AQUA and PROCHECK-NMR: programs for checking the quality of protein structures solved by NMR. J. Biomol. NMR *8*, 477–486.

Laubacher, M.E., and Ades, S.E. (2008). The Rcs phosphorelay is a cell envelope stress response activated by peptidoglycan stress and contributes to intrinsic antibiotic resistance. J. Bacteriol. *190*, 2065–2074.

Levit, M.N., Liu, Y., and Stock, J.B. (1999). Mechanism of CheA protein kinase activation in receptor signaling complexes. Biochemistry *38*, 6651–6658.

Linge, J.P., Williams, M.A., Spronk, C.A., Bonvin, A.M., and Nilges, M. (2003). Refinement of protein structures in explicit solvent. Proteins *50*, 496–506.

Majdalani, N., and Gottesman, S. (2005). The Rcs phosphorelay: a complex signal transduction system. Annu. Rev. Microbiol. *59*, 379–405.

Majdalani, N., Heck, M., Stout, V., and Gottesman, S. (2005). Role of RcsF in signaling to the Rcs phosphorelay pathway in *Escherichia coli*. J. Bacteriol. *187*, 6770–6778.

Maris, A.E., Kaczor-Grzeskowiak, M., Ma, Z., Kopka, M.L., Gunsalus, R.P., and Dickerson, R.E. (2005). Primary and secondary modes of DNA recognition by the NarL two-component response regulator. Biochemistry *44*, 14538–14552.

McEvoy, M.M., Muhandiram, D.R., Kay, L.E., and Dalquist, F.W. (1996). Structure and dynamics of a CheY-binding domain of the chemotaxis kinase CheA determined by nuclear magnetic resonance spectroscopy. Biochemistry *35*, 5633–5640.

Miller, J.F. (1972). Experiments in Molecular Genetics (Cold Spring Harbor, NY: Cold Spring Harbor Laboratory).

Moseley, H.N., Monleon, D., and Montelione, G.T. (2001). Automatic determination of protein backbone resonance assignments from triple resonance nuclear magnetic resonance data. Methods Enzymol. *339*, 91–108.

Mourey, L., Da Re, S., Pedelacq, J.D., Tolstykh, T., Faurie, C., Guillet, V., Stock, J.B., and Samama, J.P. (2001). Crystal structure of the CheA histidine phosphotransfer domain that mediates response regulator phosphorylation in bacterial chemotaxis. J. Biol. Chem. *276*, 31074–31082.

Nixon, B.T., Ronson, C.W., and Ausubel, F.M. (1986). Two-component regulatory systems responsive to environmental stimuli share strongly conserved domains with the nitrogen assimilation regulatory genes ntrB and ntrC. Proc. Natl. Acad. Sci. USA *83*, 7850–7854.

Pristovsek, P., Sengupta, K., Löhr, F., Schäfer, B., von Trebra, M.W., Rüterjans, H., and Bernhard, F. (2003). Structural analysis of the DNA-binding domain of the *Erwinia amylovora* RcsB protein and its interaction with the RcsAB box. J. Biol. Chem. *278*, 17752–17759.

Reese, M.L., and Dotsch, V. (2003). Fast mapping of protein-protein interfaces by NMR spectroscopy. J. Am. Chem. Soc. *125*, 14250–14251.

Robinson, V.L., Buckler, D.R., and Stock, A.M. (2000). A tale of two components: a novel kinase and a regulatory switch. Nat. Struct. Biol. *7*, 626–633.

Rogov, V.V., Bernhard, F., Lohr, F., and Dotsch, V. (2004). Solution structure of the *Escherichia coli* YojN histidine-phosphotransferase domain and its interaction with cognate phosphoryl receiver domains. J. Mol. Biol. *343*, 1035–1048.

Rogov, V.V., Rogova, N.Y., Bernhard, F., Koglin, A., Lohr, F., and Dotsch, V. (2006). A new structural domain in the *Escherichia coli* RcsC hybrid sensor kinase connects histidine kinase and phosphoreceiver domains. J. Mol. Biol. *364*, 68–79.

Rogov, V.V., Löhr, F., Rogova, N., Klammt, C., Koglin, A., Bernhard, F., and Dötsch, V. (2007). NMR assignment of 1H, 13C and 15N resonances of the truncated *Escherichia coli* RcsC (700-949), including the phosphoreceiver domain. J. Biomol. NMR *38*, 165.

Stephenson, K., and Hoch, J.A. (2002). Evolution of signalling in the sporulation phosphorelay. Mol. Microbiol. *46*, 297–304.

Stewart, R.C. (1997). Kinetic characterization of phosphotransfer between CheA and CheY in the bacterial chemotaxis signal transduction pathway. Biochemistry *36*, 2030–2040.

Stewart, R.C., and Van Bruggen, R. (2004). Association and dissociation kinetics for CheY interacting with the P2 domain of CheA. J. Mol. Biol. *336*, 287–301.

Stock, J.B., Ninfa, A.J., and Stock, A.M. (1989). Protein phosphorylation and regulation of adaptive responses in bacteria. Microbiol. Rev. *53*, 450–490.

Takeda, S., Fujisawa, Y., Matsubara, M., Aiba, H., and Mizuno, T. (2001). A novel feature of the multistep phosphorelay in E*scherichia coli*: a revised model of the RcsC → YojN → RcsB signalling pathway implicated in capsular synthesis and swarming behaviour. Mol. Microbiol. *40*, 440–450.

Tomomori, C., Tanaka, T., Dutta, R., Park, H., Saha, S.K., Zhu, Y., Ishima, R., Liu, D., Tong, K.I., Kurokawa, H., et al. (1999). Solution structure of the homodimeric core domain of *Escherichia coli* histidine kinase EnvZ. Nat. Struct. Biol. *6*, 729–734.

Uhl, M.A., and Miller, J.F. (1996). Central role of the BvgS receiver as a phosphorylated intermediate in a complex two-component phosphorelay. J. Biol. Chem. *271*, 33176–33180.

Varughese, K.I., Tsigelny, I., and Zhao, H. (2006). The crystal structure of berylloflfluoride Spo0F in complex with the phosphotransferase Spo0B represents a phosphotransfer pretransition state. J. Bacteriol. *188*, 4970–4977.

Wehland, M., and Bernhard, F. (2000). The RcsAB box. Characterization of a new operator essential for the regulation of exopolysaccharide biosynthesis in enteric bacteria. J. Biol. Chem. *275*, 7013–7020.

Wehland, M., Kiecker, C., Coplin, D.L., Kelm, O., Saenger, W., and Bernhard, F. (1999). Identification of an RcsA/RcsB recognition motif in the promotors of exopolysaccharide biosynthetic operons from *Erwinia amylovora* and *Pantoea stewartii* subspecies stewartii. J. Biol. Chem. *274*, 3300–3307.

West, A.H., and Stock, A.M. (2001). Histidine kinases and response regulator proteins in two-component signaling systems. Trends Biochem. Sci. *26*, 369–376.

Wishart, D.S., Bigam, C.G., Yao, J., Abildgaard, F., Dyson, H.J., Oldfield, E., Markley, J.L., and Sykes, B.D. (1995). 1H, 13C and 15N chemical shift referencing in biomolecular NMR. J. Biomol. NMR *6*, 135–140.

Xu, Q., Porter, S.W., and West, A.H. (2003). The yeast YPD1/SLN1 complex: insights into molecular recognition in two-component signaling systems. Structure *11*, 1569–1581.

Zapf, J., Sen, U., Madhusudan, Hoch, J.A., and Varughese, K.I. (2000). A transient interaction between two phosphorelay proteins trapped in a crystal lattice reveals the mechanism of molecular recognition and phosphotransfer in signal transduction. Structure *8*, 851–862.

Zhang, W., and Shi, L. (2005). Distribution and evolution of multiple-step phosphorelay in prokaryotes: lateral domain recruitment involved in the formation of hybrid-type histidine kinases. Microbiology *151*, 2159–2173.

Zhao, X., Copeland, D.M., Soares, A.S., and West, A.H. (2008). Crystal structure of a complex between the phosphorelay protein YPD1 and the response regulator domain of SLN1 bound to a phosphoryl analog. J. Mol. Biol. *375*, 1141–1151.

Zhou, H., McEvoy, M.M., Lowry, D.F., Swanson, R.V., Simon, M.I., and Dahlquist, F.W. (1996). Phosphotransfer and CheY-binding domains of the histidine autokinase CheA are joined by a flexible linker. Biochemistry *35*, 433–443.